PCCP

Cite this: *Phys. Chem. Chem. Phys.*, 2011, **13**, 16254–16264

www.rsc.org/pccp

**PAPER**

# Trends in structural, electronic and energetic properties of bimetallic vanadium–gold clusters $Au_nV$ with $n = 1$–14†

**Pham Vu Nhat**[ab] **and Minh Tho Nguyen***[ac]

***Received 25th June 2011, Accepted 19th July 2011***
**DOI: 10.1039/c1cp22078k**

A systematic quantum chemical investigation on the electronic, geometric and energetic properties of $Au_nV$ clusters with $n = 1$–14 in both neutral and anionic states is performed using BP86/cc-pVTZ-PP calculations. Most clusters having an even number of electrons prefer a high spin state. For odd-electron systems, a quartet state is consistently favoured as the ground state up to $Au_8V$. The larger sized $Au_{10}V$, $Au_{12}V$ and $Au_{14}V$ prefer a doublet state. The clusters prefer 2D geometries up to $Au_8V$ involving a weak charge transfer. The larger systems bear 3D conformations with a more effective electron transfer from Au to V. The lowest-energy structure of a size $Au_nV$ is built upon the most stable form of $Au_{n-1}V$. During the growth, V is endohedrally doped in order to maximize its coordination numbers and augment the charge transfer. Energetic properties, including the binding energies, embedding energies and second-order energy differences, show that the presence of a V atom enhances considerably the thermodynamic stability of odd-numbered gold clusters but reduces that of even-numbered systems. The atomic shape has an apparently more important effect on the clusters stability than the electronic structure. Especially, if both atomic shape and electronic condition are satisfied, the resulting cluster becomes particularly stable such as the anion $Au_{12}V^-$, which can thus combine with the cation $Au^+$ to form a superatomic molecule of the type $[Au_{12}V]Au$. Numerous lower-lying electronic states of these clusters are very close in energy, in such a way that DFT computations cannot clearly establish their ground electronic states. Calculated results demonstrate the existence of structural isomers with comparable energy content for several species including $Au_9V$, $Au_{10}V$, $Au_{13}V$ and $Au_{14}V$.



## 1. Introduction

Gold clusters constitute an interesting research field owing to their potential applications in nanoscale devices,[1] and their unique catalytic activities supported by such nano-particles,[2] contrary to the particular inertness of the gold bulk. In this context, clusters of gold have been the subject of continuing experimental and theoretical investigations. Electron affinities, vertical detachment energies and ionization energies of small to medium sized gold clusters were evaluated in early experiments.[3–5] Rate constants and monomer–dimer branching ratios for decays of gold cluster cations were also measured.[6] Recently, Gruene and co-workers[7] were able to record the vibrational spectra of neutral clusters $Au_7$, $Au_{19}$ and $Au_{20}$ in the gas phase. From experimental photoelectron spectra, $Au_{20}$ was confirmed to be a tetrahedron and hold a particularly large HOMO–LUMO gap which is even larger than that of $C_{60}$.[8] Besides, numerous theoretical studies were carried out on various aspects of geometrical, electronic and thermodynamic properties of neutral and ionic gold clusters.[9–16] One of the key findings is the preference for planar structures of small sizes, and the crossover from planarity to non-planarity is found to occur at the size of $Au_{13}$ for neutrals.[15] Concerning the cations $Au_n^+$ and anions $Au_n^-$, the 2D–3D transition occurs at a size of $n \approx 7$ and $n \approx 11$–12, respectively.[11–14,16] A widely accepted explanation for such a remarkable difference is based on strong relativistic effects,[17,18] which compact the size of s atomic orbitals, and subsequently enhance the s–d hybridization and d–d interaction, leading to a preference for more directional Au–Au bonds.[19–22]

From previous investigations performed on the doped gold clusters, with dopant atoms ranging from light elements to transition metals, the impurity atoms strongly influence the physical and chemical properties of host gold systems. For example, $Au_4Si$ prefers a platonic solid $T_d$ structure,[23] instead of a 2D shape such as that of $Au_5$, and is exceptionally stable.[24] Similarly, $Au_5M$ clusters, in which dopant atoms M are p elements such as Al, Si and P,[25] also exhibit non-planar structures, moving away from the typical planar triangular form of $Au_6$.[9] More remarkably, even though neither the 13-atom gold neutral nor its charged species favor a high

[a] *Department of Chemistry, Katholieke Universiteit Leuven, B-3001 Leuven, Belgium. E-mail: minh.nguyen@chem.kuleuven.be*
[b] *Department of Chemistry, Can Tho University, Can Tho, Vietnam*
[c] *Institute for Computational Science and Technology of HoChiMinh City, Thu Duc, HoChiMinh City, Vietnam*

† Electronic supplementary information (ESI) available. See DOI: 10.1039/c1cp22078k

 

symmetry icosahedral ($I_h$) structure,[15,26] a number of icosahedral clusters $Au_{12}M$, in which the impurity atom is normally a transition metal, have been found. In fact, the existence of platonic solid $I_h$ clusters $Au_{12}M^x$ with $M^x = V^-$, $Nb^-$, Ta, $Ta^-$, W, $Re^+$ was theoretically predicted and experimentally confirmed by several groups.[27–30] These clusters are unique as they possess an exceptionally high thermodynamic stability and a particularly large frontier orbital energy gap.[31] The measured vertical electron detachment energies (VDEs) for anions $Au_{12}V^-$, $Au_{12}Nb^-$ and $Au_{12}Ta^-$ amount to 3.79, 3.88 and 3.90 eV,[28] respectively, as compared to that of 3.94 eV of $Au_{13}^-$.[32]

Especially, a series of iso-electronic gold-caged neutrals $Au_{14}M$ (M = Zr, Hf) and anions $Au_{14}M^-$ (M = Sc, Y) are predicted to have HOMO–LUMO gaps even larger than those of $Au_{12}W$ and $Au_{20}$ clusters, which hold a large measured gap of $>1.6$ eV.[33] Several groups also investigated the anionic $Au_{16}^-$ cage encapsulating Cu, Fe, Co, Ni, Ag, Zn, In *etc.* species, and confirmed that the impurity greatly modifies the geometric and electronic properties of the host.[34–36] Recently, a combined study using FIR-MPD vibrational spectroscopy and quantum chemical calculations allowed Lin and co-workers to determine the lowest-energy structures of a series of small yttrium-doped gold $Au_nY$ ($n$ = 1–9) clusters.[37] It turns out that these clusters differ from pure gold clusters and favor non-planar geometries already from $Au_4Y$. In addition, the presence of Y tends to enhance considerably the thermodynamic stability of the binary clusters.

In contrast to the well-developed understanding of pure gold clusters, there is relatively less information available about structural and electronic properties of bimetallic gold–vanadium systems. Our knowledge on combinations between gold and vanadium elements is restricted on some discrete sizes such as $Au_6V^{0/-}$,[38,39] $Au_{12}V^-$,[28,31,40] and $Au_{24}V$,[41] and a more systematic investigation on the cations $Au_nV^+$ ($n$ = 1–9) by Torres and co-workers.[42] These reports do not allow us to have a view on the mixed V and Au species. In this context, we set out to theoretically investigate a series of small vanadium-doped gold clusters $Au_nV$ with $n$ = 1–14 in order to probe systematically their behavior and the evolution of their structural, electronic and energetic properties. The basic energetic properties, *i.e.* electron affinities (EA), ionization energies (IE), dissociation energies ($D_e$), and binding energy per atom (BE), as a function of cluster sizes are determined and calibrated from available experimental data. In addition, the calculated results obtained for doped systems are compared with those of pure gold systems in order to evaluate the effects of impurity on the host clusters. The main purposes of this study are thus to identify the lowest-energy structures as well as the general trends in the size-dependent stability and growth of bimetallic clusters $Au_nV$ in both neutral and anionic states.

## 2. Computational methods

All electronic structure calculations are carried out using the Gaussian 09 suite of program.[43] The plausible geometries for all sizes of $Au_nV$ are initially investigated making use of DFT with the pure BP86 functional and the effective core potential LANL2DZ basis set. Subsequently, geometries of the most relevant lower-lying isomers are reoptimized utilizing the correlation consistent cc-pVTZ-PP basis set,[44] where PP stands for a pseudo-potential. This basis set with effective core potential (ECP) already includes the relativistic effects that are crucial in the treatment of heavy elements such as gold. For the gold element, the basis set employed includes nineteen electrons on 5s, 5p, 5d, 6s orbitals as valence electrons, while those of vanadium comprise thirteen electrons on the 4s, 4p, 4d, 5s orbitals. The spin multiplicity of a specific size is considered at 1 (singlet), 3 (triplet) and 5 (quintet) for even-electron clusters and 2 (doublet), 4 (quartet) and 6 (sextet) for odd-electron clusters.

The initial structures for geometry optimizations are constructed *via* two routes. In the first one whose procedure can also be called 'successive growth algorithm', the initial geometries of a certain size $Au_nV$ are generated from the lowest-lying isomers of the smaller size $Au_{n-1}V$ by adding an extra Au atom randomly. In the second route, we employ previous results on related transition metal clusters as a guide, in particular we use the lower-lying structure of the pure gold clusters $Au_{n+1}$ to generate the structure of $Au_nV$ by substitution of one Au by V. A genetic algorithm code is also used but it is extremely computer time-consuming and does not lead to better results. Harmonic vibrational frequencies are subsequently computed to confirm that the optimized geometries correspond to local minima or transition states on the potential energy surface.

In order to calibrate the computed results, we perform density functional theory calculations on the diatomic clusters $Au_2$ and AuV using the popular pure BP86, hybrid B3LYP and hybrid meta-GGA M06 functionals, in conjunction with the cc-pVTZ-PP basis set. The calculated results are presented in Table 1, along with available experimental data. For $Au_2$, the calculated bond length increases in the order BP86 < B3LYP < M06, and likely overestimate the experimental value by ~0.05 (BP86), 0.08 (B3LYP) to 0.10 Å (M06). Similarly, the BP86 functional consistently predicts the shortest equilibrium ($r_e$) distance for AuV, while the M06 gives the longest one. There is no experimental result for the mixed diatomic species. Note that the experimental value is the vibrationally averaged distance ($r_0$). The calculated $D_e$ values

**Table 1** Theoretical and experimental results of bond length $R_e$ (Å), dissociation energy $D_e$ (eV), ionization energy IE (eV), electron affinity EA (eV) and vibrational frequency $\omega_e$ ($cm^{-1}$) for $Au_2$ and AuV

| | | Calculation | | | |
|---|---|---|---|---|---|
| Species | Property | BP86 | B3LYP | M06 | Experiment |
| $Au_2$ | $R_e$ | 2.520 | 2.547 | 2.575 | 2.472[a] |
| | $D_e$ | 2.27 | 1.96 | 2.17 | 2.29 ± 0.02[a] |
| | IE | 9.58 | 9.33 | 9.15 | 9.20 ± 0.21[b] |
| | EA | 2.08 | 1.89 | 1.77 | 1.92[c] |
| | $\omega_e$ | 173 | 167 | 160 | 191[a] |
| AuV | $R_e$ | 2.465 | 2.512 | 2.528 | |
| | $D_e$ | 2.71 | 2.41 | 2.31 | 2.51 ± 0.09[a] |
| | IE | 7.30 | 7.03 | 7.08 | |
| | EA | 1.17 | 1.10 | 1.41 | |
| | $\omega_e$ | 231 | 219 | 212 | |

[a] Ref. 45. [b] Ref. 46. [c] Ref. 32.

of $Au_2$ are ~2.3 (BP86), 2.0 (B3LYP) and 2.2 eV (M06) as compared to the experimental value of 2.29 ± 0.02 eV.[45] The BP86 functional appears to provide a better result for this quantity. Concerning AuV, the predicted $D_e$ obtained from B3LYP is however apparently in closer agreement with the experiment. For ionization energies, the M06 prediction for $Au_2$ deviates by ~0.05 eV from the measured value,[46] while B3LYP and BP86 values differ by ~0.13 and 0.38 eV from it, respectively. In contrast, the EA of $Au_2$ obtained with the BP86 is closer to the experiment[32] than other methods. Although it appears to be difficult to judge on the absolute accuracy of the results obtained by these DFT methods, the BP86 functional provides in general for this type of compounds a more consistent set of data.

The assessment of the performance of the BP86 functional for transition metal compounds has abundantly been reported in the literature.[47] Although each functional naturally has its own advantages and drawbacks for different properties, the BP86 describes relatively well the electronic, geometric, spectroscopic and energetic properties of transition-metal compounds. Barden *et al.*[48] applied the LSDA, BP86, BLYP, B3P86, and B3LYP functionals to nine homonuclear 3d dimers and found that the mean unsigned error for bond distances obtained by BP86 is only around 0.02 Å as compared to 0.053 Å of B3LYP. Li and Dixon[49] used experimental electron detachment energies for $MO_6^-$ (M = Cr, Mo, and W) and $M_2O_6^-$ (M = Cr and W) to test the predictions of CCSD(T) and 28 functionals. These authors found that the BP86 agrees best with the experiment, with a maximum error of 0.29 eV and second largest absolute error of 0.07 eV; CCSD(T) had a maximum and second largest absolute error of 0.31 and 0.12 eV, respectively. The functional was also proved to be applicable in predicting bond dissociation energy of 3d transition metal carbonyls.[50] Stevens and co-workers[51] applied two LSDAs, seven GGAs, seven meta GGAs, and four hybrid GGAs to bond distances, vibrational frequencies, and dipole moments of diatomics of Cr, Mo, and W with C, N, and O. The BP86 functional is again judged to be the most satisfactory. Song *et al.*[52] applied one LSDA, three GGAs, and five hybrid GGAs to bond energies, bond lengths, and vibrational frequencies of 20 4d-series neutral and cationic monoxides. The main conclusions about performance are based on bond energies of neutrals, and the BP86 functional, along with BLYP and BPW91 functionals, is confirmed to yield the most reliable results. Therefore we selected the pure functional BP86 for most calculations carried out in this study. Unless otherwise stated, the values mentioned hereafter are obtained from BP86/cc-pvTZ-PP calculations. For energetic parameters, zero-point energy corrections are also included.

## 3. Results and discussion

As for a convention, the structures considered are denoted as ***n*–*X*** where ***n*** is the cluster size ranging from 1 to 14, and ***X*** = **I**, **II**, **III** *etc.* are the number of isomers located. The letter GS stands for the ground electronic state.

### 3.A. Equilibrium structures of the neutrals and the growth mechanism

The lowest-energy structures of bimetallic clusters $Au_nV$ are presented in Fig. 1 and 2. They adopt planar forms up to $n$ = 8, and a 2D–3D transition apparently occurs at $n$ = 9. Clusters larger than $Au_9V$ tend to form 3D structures, in which the V atom is endohedrally doped to maximize its coordination number. From a growth mechanism point of view, we find that the replacement of one Au in the $Au_{n+1}$ species by one V atom to form $Au_nV$ complexes generally results in a significant structural rearrangement. Except for $Au_2V$ and $Au_4V$, the doped $Au_nV$ and the pure $Au_{n+1}$ clusters bear a completely different shape in their ground state. The shapes of the doped clusters are described in some detail in the following sections.

**AuV.** The GS of the smallest species AuV is a quintet state with the orbital configuration $^5\sum^+$:...$(2\sigma)^2(3\delta)^1(2\pi)^1(2\pi)^1(3\sigma)^1$. The highest singly occupied orbital (SOMO) σ (given in Fig. S1 of the ESI†) is an anti-bonding orbital and mainly of 4s, $3d_{z^2}$ (V). Other singly occupied orbitals are two π and one δ MOs. They all have anti-bonding character and are largely contributed from V(d: $d_{xz}$, $d_{yz}$, $d_{xy}$) orbitals as well. Hence, four

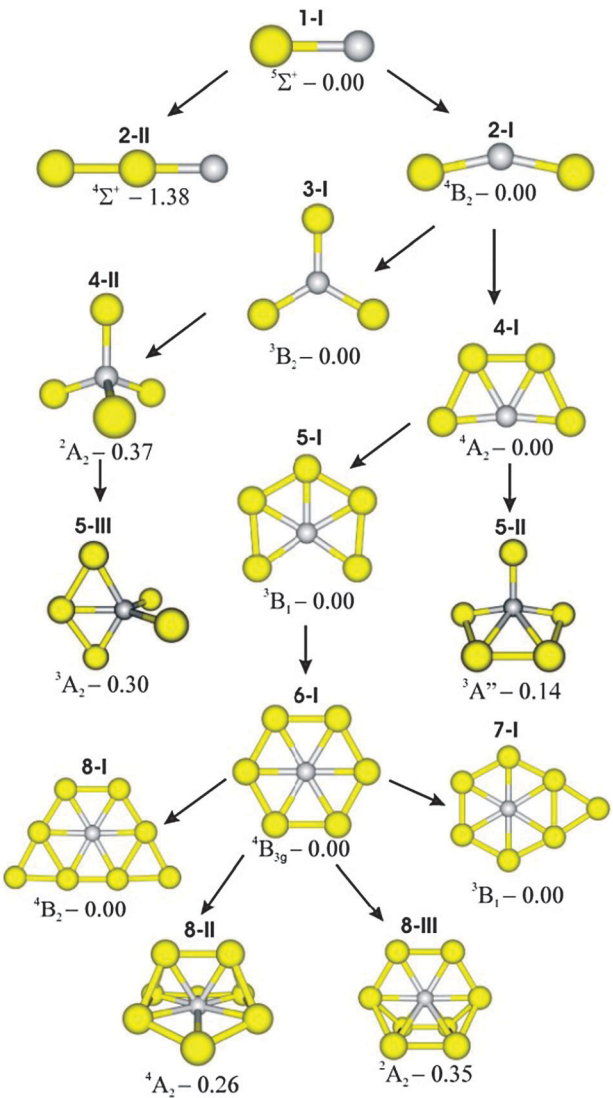


**Fig. 1** Lower-lying structures considered for $Au_nV$ clusters ($n \leq 8$) and their relative energies at the BP86/cc-pVTZ-PP + ZPE level. Arrows are the proposed evolution routes.

 

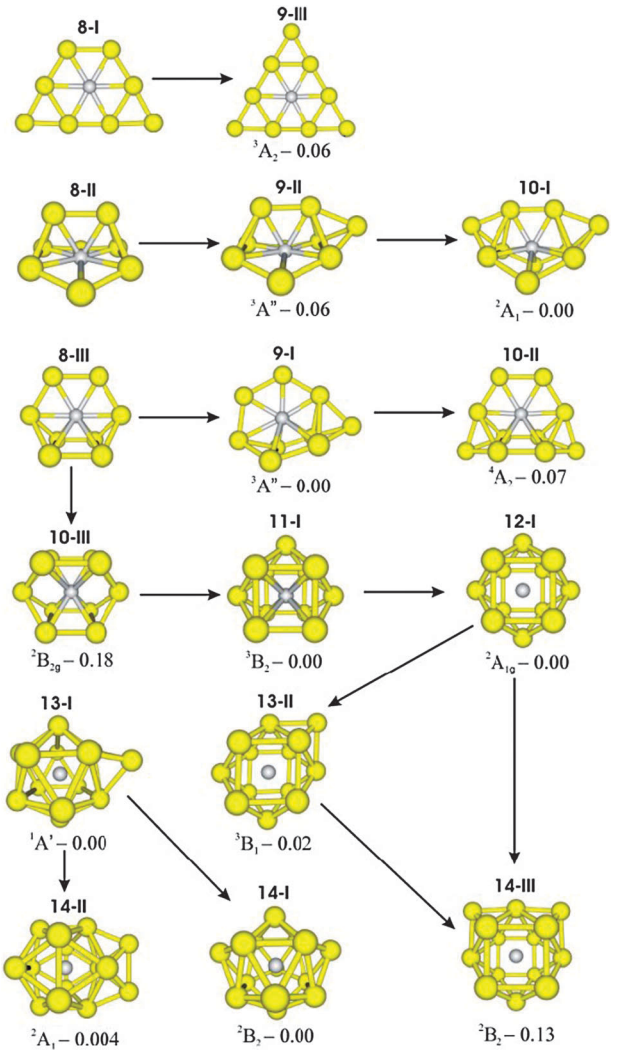


**Fig. 2** Lower-lying structures considered for $Au_nV$ clusters ($n$ = 8–14) and their relative energies at the BP86/cc-pVTZ-PP + ZPE level.

unpaired electrons are mostly located on the d(V) orbitals. The interaction that forms chemical bonding in AuV occurs between the $3d_{z^2}$, $3d_{xz}$, $3d_{yz}$, 4s AOs of V and the same symmetry counterparts of Au, giving rise to 1σ, 1π and 2σ bonding orbitals. The lower spin singlet and triplet states are 2.42 and 0.97 eV above GS, respectively. The optimal bond length Au–V varies from 2.47 (BP86), 2.53 (M06) to 2.54 Å (B3LYP), while that of $Au_2$ covers the range from 2.52 (BP86), 2.55 (B3LYP) to 2.58 Å (M06). Replacement of Au by V thus leads to a mild decrease of bond length. In addition, due to the larger EA of the Au element (2.31 eV) than that of V (0.53 eV),[46,53] the Au–V bond is relatively ionic with a positive charge centered at V (+0.42 electron).

**$Au_2V$.** The lowest-energy structure of the trimer $Au_2V$ is a $C_{2v}$ form **2–I** with a $^4B_2$ GS, and an equilibrium Au–V distance of *ca.* 2.44 Å. The latter is slightly shorter than those in AuV (~2.47 Å) and in $Au_3$ (2.55 Å) computed at the BP86/cc-pVTZ-PP level. The low-spin $^2B_2$ state of this form lies 0.68 eV above GS. Another stable structure obtained for $Au_2V$ is the linear **2–II**, which also prefers to stay in a high spin state $^4\sum^+$, and is *ca.* 0.23 eV above the $^4B_2$ GS. As the GS of the vanadium atom possesses a $[Ar]3d^34s^2$ configuration, it consequently uses nine orbitals of 3d, 4s and 4p shells that are available for making chemical bonds. In addition, empty d AOs of V can act as electron acceptors by combining with orbitals of the gold backbone. Therefore, $Au_nV$ is expected to be more stabilized if the coordination number of V is getting higher. Indeed, isomer **2–I** in which the V atom has a coordination number of two is much more stable than **2–III** (by ~1.4 eV), in which V has a coordination number of one.

**$Au_3V$.** In terms of crystal filed theory, when placed in a $D_{3h}$ ligand field, five d orbitals of V will split into three levels as follows:

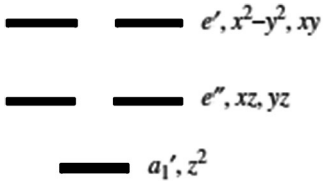


Thus, starting from the higher symmetry $D_{3h}$ structure, $Au_3V$ with four d electrons and a triplet state will have had two electrons in $a_1'$, one in e″ and the other in e′. In this case, the energy of the $a_1'$ orbital is substantially lower than those of e″ and e′ orbitals which are very close in energy. Hence, a triplet state is favoured over the singlet or quintet states. However such a degenerate state is not stable upon Jahn–Teller distortions and the molecule undergoes a geometry relaxation to remove that degeneracy. The resulting stable structure **3–I** of $Au_3V$ is thus vaguely distorted from $D_{3h}$ to $C_{2v}$ with the V atom occupying a central position. Again, this system also prefers a high-spin $^3B_2$ GS, and the quasi-degenerate $^3A_1$ state is only 0.06 eV higher. The shapes and symmetries of frontier molecular orbitals in $Au_3V$, giving rise from the interactions between valence AOs of V and Au atoms, are shown in Fig. S2 of ESI.† It is clear that, of five d V AOs, only $3d_{z^2}$ is not involving in bonding orbitals. The interactions between other 3d V AOs with the symmetry-matching ligand orbitals yield $b_2$, $a_1$, $a_2$ and $b_1$ bonding and anti-bonding MOs. Two unpaired electrons are located in anti-bonding MOs with $b_1$ and $a_2$ symmetries. Previously, Lin *et al.*[37] found that the tetramer $Au_3Y$ exhibits an ideal $D_{3h}$ form, as it possesses a $^1A_1'$ GS.

**$Au_4V$.** The most stable form **4–I**, with the $C_{2v}$ point group and the $^4A_2$ GS, is built up either from replacing one Au in GS of $Au_5$[54–56] by V, or from attaching one Au atom to **3–I**. The low-spin $^2A_1$ state of this form is less favored than GS by 0.57 eV. The first 3D structure **4–II**, which is distorted from a tetrahedral to $C_{2v}$ symmetry, has a $^2A_2$ state and is 0.37 eV higher in energy.

**$Au_5V$.** Three structures **5–I**, **5–II** and **5–III** are predicted to be the most stable forms of the hexameric cluster, in which **5–I** can be considered as arising from addition of one Au atom to the lowest-energy isomer of the pentamer **4–I**, while **5–II** is greatly distorted from a $D_{5h}$ shape. The GS is a $^3B_1$ state of **5–I**. Both triplet $^3B_2$ and $^3A_2$ states of **5–II** and **5–III** are energetically less favorable by 0.14 and 0.30 eV, respectively.

**$Au_6V$.** Previous investigations[38,39] suggested the most stable isomer of $Au_6V$ to be a planar structure with the V atom at the center of an $Au_6$ ring. Our calculated results concur with this finding, and in addition confirm that such geometry **6–I** with $D_{2h}$ symmetry is the most stable form of $Au_6V$. The shape of **6–I** can be viewed as generated from **5–I** by adding one Au and it now exhibits a $D_{2h}$ configuration rather than a perfect $D_{6h}$ structure. This is a result of the Jahn–Teller effect, which was thoroughly discussed by Höltzl *et al.*[57] Furthermore, our DFT calculations record two quasi-degenerate states $^4B_{3g}$ and $^4B_{2g}$ competing to be the GS of $Au_6V$. Using the BP86 functional in conjunction with the cc-pVTZ-PP basis set, the $^4B_{2g}$ state is found to be only 0.03 eV higher than the $^4B_{3g}$ state. The lower spin state $^2B_{3g}$ of this form is located at 0.17 eV higher in energy than the $^4B_{3g}$ state. The two next lower-lying isomers are **6–II** and **6–III**, in which the former can be viewed as a result of substituting one Au in GS of $Au_7$,[15] while the latter bears a 3D structure and significantly less stable by $\sim$0.26 eV above GS. Other local minima, which are much higher in energy, are displayed in Fig. S2 of the ESI.†

**$Au_7V$.** The global minimum of $Au_7V$ is still a planar $C_{2v}$ configuration **7–I** and a $^3B_1$ GS. As preceding systems, this cluster is built upon the most stable isomer of the smaller size **6–I** by capping one Au, in which the latest Au is attached to an edge of the $Au_6$ ring. The second most stable isomer **7–II** has a $C_{2v}$ 2D as well. Its $^3B_1$ state is 0.18 eV less stable than GS. We also find several 3D structures for the octamer $Au_7V$, but they are much less stable than the 2D counterparts. Their geometries, point groups, electronic states and relative energies (at the BP86/LanL2DZ level) are summarized in Fig. S3 of ESI.†

**$Au_8V$.** Continuous addition of one Au atom to the lowest-energy structure **7–I** yields the most stable form **8–I**. The high spin $^4B_2$ state of **8–I** is predicted to be GS, while the corresponding low-spin $^2B_2$ state is less stable by $\sim$0.30 eV. Other local minima **8–II** and **8–III** have 3D structures and can be considered as formed from addition of two gold atoms to the lowest-energy **6–I**. However, such forms are relatively less stable than the 2D shaped **8–I**. In fact, the $^4A_2$ state of **8–II** and the $^2A_2$ of **8–III** are 0.26 and 0.35 eV above the GS, respectively.

**$Au_9V$.** At the BP86/cc-pVTZ-PP level of theory, we find three quasi-isoenergetic structures **9–I**, **9–II** and **9–III** competing for GS of $Au_9V$. Interestingly, they are all obtained by adding an extra Au atom to the three lowest-lying structures of $Au_8V$ (see above). The **9–I** corresponds to the third most stable **8–III** isomer, while **9–II** and **9–III** come from **8–II** and **8–I**, respectively. Furthermore, the BP86 functional predicts **9–I** with a $^3A''$ state as GS of $Au_9V$, and two nearly-degenerate states $^3A''$ (**9–II**) and $^3A_2$ (**9–III**) are only marginally located above (0.06 eV).

**$Au_{10}V$.** As mentioned above, small gold clusters as well as their anionic and cationic clusters tend to prefer planar geometries, and so are several transition metal doped derivatives. Previous investigations on $Au_nTi$[58] recorded a 2D–3D transition at $n = 8$. For $Au_nV$ systems, we find that the crossover from planarity to non-planarity is initiated at $Au_9V$. Indeed, $Au_{10}V$ represents the first size considered in the present study whose lowest-energy conformation does not have a two-dimensional shape. The three most stable isomers of $Au_{10}V$, *i.e.* **10–I**, **10–II** and **10–III**, are all non-planar and exhibit low spin GS. Isomers **10–II** ($^4A_2$) and **10–III** ($^2B_{2g}$) are evaluated to be 0.07 and 0.18 eV, respectively, above **10–I** ($^2A_1$). However, it is worth noting that the latter structure is the lowest-energy isomer of anion $Au_{10}V^-$ and constitutes a cornerstone for larger sizes as well.

**$Au_{11}V$.** The most stable structure **11–I** is an incomplete cuboctahedron with a $C_{2v}$ point group and high spin $^3B_2$ state. Such a form is acquired by capping a gold atom on **10–III** rather than on **10–I** or **10–II**. A growth path from **10–II** leads to **11–II**, whereas the route going from the most stable **10–I** actually yields **11–III** (*cf.* Fig. S3 of ESI†). These structures are much less stable than **11–I**. In fact, the $^3A_2$ state of **11–II** and $^3B_1$ of **11–III** are predicted to be $\sim$0.46 and $\sim$1.13 eV above the $^3B_2$ GS of **11–I**.

**$Au_{12}V$.** Starting from **11–I** and adding an extra Au, we obtain the GS **12–I**. Previously, the $I_h$ icosahedral structure of the anion $Au_{12}V^-$ was reported to be significantly preferred over the $O_h$ cuboctahedron.[28,31] In addition, its HOMO is 5-fold degeneracy ($h_g$) with 10 electrons and the anion has a closed-shell $^1A_{1g}$ state.[40] Hence, removal of an electron from the ideal icosahedron $Au_{12}V^-$ to form the neutral $Au_{12}V$ is expected to reduce the molecular symmetry due to the Jahn–Teller effect. Cuboctahedra and icosahedra are very closely related as they can easily be interconverted.[59] Thus, the distortion of this icosahedron leads to a cuboctahedron. However, **12–I** is characterized by a slightly distorted cuboctahedron with a $D_{4h}$ point group, instead of a perfect $O_h$ form, as it possesses an open-shell but low spin electronic configuration ($^2A_{1g}$). Previously, it was found that all open-shell $Au_{12}M$ species, where M is a 5d transition element from Hf to Hg, and closed-shell $Au_{12}Hg$, also energetically favor the $O_h$ geometry, whereas for closed-shell $Au_{12}W$, both $O_h$ and $I_h$ forms are nearly isoenergetic.[60]

**$Au_{13}V$.** From attachment of one gold atom to an icosahedron or cuboctahedron, two different isomers **13–I** and **13–II** are built upon. Nevertheless, they possess a tiny energy difference, in which the low spin $^1A'$ state of **13–I** is only marginally $\sim$0.02 eV below the high-spin $^3B_1$ state of **13–II**. They are thus energetically degenerate. It can be seen that **13–II** is obtained from a pathway, which is called a successive growth algorithm,[61] through the most stable **12–I**. In contrast, **13–I** can be viewed as a super-atomic molecule, containing both $Au_{12}V^-$ and $Au^+$ units. Indeed, NBO analysis shows that the $Au_{12}V$ moiety bears a partially negative charge of $-0.26$ electron, and the capping gold atom has a positive charge of $+0.26$ electron. Likewise, **11–I** can also be considered as a super-atomic molecule constituted from both $Au_{10}V^-$ and $Au^+$ parts. In this case, the capping Au has a positive charge of $+0.34$ electron. Another superatomic molecule of transition metal clusters was recently recorded for $Cu_{17}Sc$, whose constituents are $Cu_{16}Sc^+$ and $Cu^-$.[62]

**$Au_{14}V$.** Again, DFT computations detect two isoenergetic structures, namely **14–I** and **14–II**. **14–I**, in which V is encapsulated in a hollow cage formed by 14 gold atoms, is very similar to those of $Au_{14}M$ with M = Ti, Zr, Hf,[33,63] while

 

**14–II** is given rise from attaching one Au to **13–I**. Even though their geometries are much different from each other, they are extremely close in energy; each of the two forms can emerge as GS. Indeed, BP86/cc-pVTZ-PP calculations predict the state $^2B_2$ of **14–I** ($D_{2d}$) and the $^2A_1$ state of **14–II** ($C_{2v}$) have the same energy context (a difference of only 0.004 eV). Another meta-stable isomer is **14–III**, which can be viewed as coming from **13–II**. The $^2B_2$ state of this $C_{2v}$ form is ~0.13 eV above GS (BP86).

### 3.B. Lowest-energy structures of anionic clusters

To determine the adiabatic electron affinities (EAs), we furthermore explore the optimal structures for the anionic $Au_nV^-$ clusters having the same sizes ($n$ = 1–14). The results for the anions are shown in Fig. 3. All energetic results are computed at the BP86/cc-pVTZ-PP level, including zero-point energy corrections.

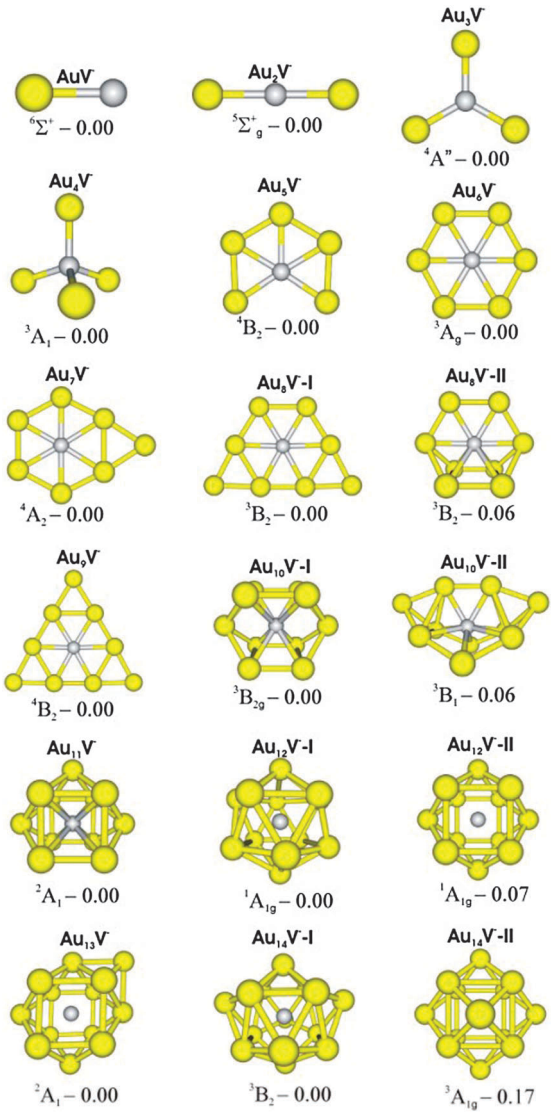


**Fig. 3** Lower-lying structures considered for the $Au_nV^-$ anions ($n$ = 1–14) and their relative energies at the BP86/cc-pVTZ-PP + ZPE level.

The BP86 functional predicts the GS of anion $AuV^-$ to be a $^6\sum^+$ state, while B3LYP and M06 reveal a $^4\sum^+$ GS. Addition of an electron to AuV ($^5\sum^+$) forming the anion $AuV^-$ ($^6\sum^+$) is predicted to increase the equilibrium distance by ~0.14 Å. In the case of $Au_2V^-$, the most stable form becomes linear, deviated from the bent like the neutral $Au_2V$. Concerning $Au_3V^-$, the minimum energy structure is not ideally planar, but it is somewhat distorted from the $C_{3v}$ point group. Similarly, reduction of $Au_4V$ to produce $Au_4V^-$ brings about a significant structural rearrangement, in which the regular tetrahedron is much more stable than all other possible isomers. Unlike the smaller species, each of the anions $Au_nV^-$ with $n$ = 5, 6, 7, 8, 11, 14 adopts the conformation identical with that of the corresponding neutral.

The remaining anions, namely $Au_9V^-$, $Au_{10}V^-$, $Au_{12}V^-$ and $Au_{13}V^-$, do not bear the same shape as their corresponding neutrals. The anion $Au_9V^-$ clearly favors a 2D structure over a 3D one, in which the isomer obtained from **9–III** is predicted to be ~0.28 eV lower in energy than that obtained from **9–I**. In the same way, the $D_{2h}$ shaped **10–III** gives rise to the most stable form for $Au_{10}V^-$.

Our result obtained for $Au_6V^-$ is also consistent with previous results by Li *et al.*[38] For the anion $Au_{12}V^-$, the $I_h$ icosahedral structure was reported to be clearly preferred over other isomers.[31] Zhai *et al.*[28] used the PW91 functional and a triple-zeta with two-polarization function (TZ2P) basis set and predicted the $O_h$ cuboctahedron to be less favored by ~0.2 eV (20.5 kJ mol$^{-1}$). In the present work at the BP86/cc-pVTZ-PP level, such isomers are evaluated with a much smaller energy difference of around ~0.06 eV (5.6 kJ mol$^{-1}$).

### 3.C. Thermodynamic stabilities

To obtain more quantitative information about the stability of $Au_nV$ clusters, we evaluate the average binding energy per atom (BE), the second-order difference of energy ($\Delta^2E$), and the embedding energy (EE). For these clusters, such parameters of a specific size are defined by the following equations:

$$\mathrm{BE} = [nE(\mathrm{Au}) + E(\mathrm{V}) - E(\mathrm{Au}_n\mathrm{V})]/(n+1)$$

$$\Delta^2E = E(\mathrm{Au}_{n+1}\mathrm{V}) + E(\mathrm{Au}_{n-1}\mathrm{V}) - 2E(\mathrm{Au}_n\mathrm{V})$$

$$\mathrm{EE} = E(\mathrm{Au}_{n-1}\mathrm{V}) + E(\mathrm{Au}) - E(\mathrm{Au}_n\mathrm{V})$$

where $E(Au_nV)$ is the energy of the lowest-lying $Au_nV$ cluster.

The graph of BEs as a function of cluster size is plotted in Fig. 4. This parameter can be regarded as the energy gained in assembling a definite cluster from isolated Au and V constituents. Generally, the chart shows a monotonic increase of BEs with respect to the cluster size. The systems tend to gain stability during the growth; larger clusters are thus more stabilized.

For the purpose of comparison, the binding energies per atom of the most stable $Au_nV$ and $Au_{n+1}$ are computed and simultaneously illustrated in Fig. 4. There have been a great number of studies on structures of small pure gold clusters.[9,10] Nevertheless, in the current work, we take the results from the most recent report,[15] in which the predicted structure of $Au_7$ is consistent with a combined experimental and theoretical

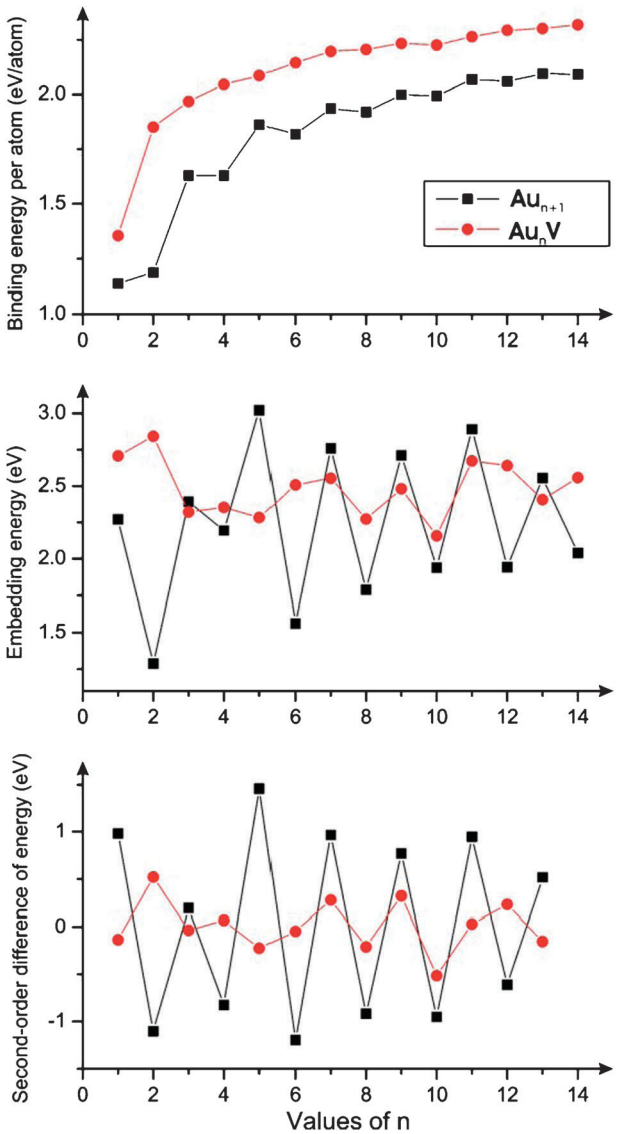


**Fig. 4** Comparison of binding energies per atom (top), embedding energies (middle) and second-order difference of energies (bottom) of $Au_{n+1}$ and $Au_nV$ as a function of cluster size. The results are obtained at the BP86/cc-pVTZ-PP + ZPE level.

vibrational investigation.[7] Optimal geometries, and then the BE values, of pure gold clusters are recomputed using the BP86/cc-pVTZ-PP level. Previously, Wang *et al.*[64] used a local density approximation to calculate the BEs up to $Au_{20}$. Experimental data have not been systematically reported yet.

As shown in Fig. 4, the BEs of the pure clusters also roughly exhibit a gradual growth and reach to the maximal value of 2.1 eV per atom for $Au_{14}$ and $Au_{15}$, whereas those of doped-clusters up to $Au_{14}V$ amount to 2.3 eV per atom. In general, the averaged binding energy of $Au_{n+1}$ is slightly smaller than that of the corresponding $Au_nV$. Let us take the dimers AuV and $Au_2$ as an example. The BE values are predicted to be 1.35 and 1.14 eV per atom, respectively, as compared to the experimental values of 1.26 ± 0.09 eV per atom for AuV and 1.15 ± 0.02 eV per atom for $Au_2$.[45] This indicates a stronger interaction between atoms in the AuV cluster as a result of the relativistic effects.

It has previously been shown that a relativistic stabilization is increased for the AuX bond if the X atom is more electropositive than gold.[65,66] Due to the fact that the electronegativity of V is smaller than that of Au, the ionic contribution to the bond Au–V is augmented by relativistic effects and, as expected, the dissociation energy is subsequently increased. Indeed, an NBO charge analysis reveals that the charge of V in $Au_2V$ is quite positive (+0.64 electron). However, for clusters larger than $Au_4V$ there exists electron back-donation from Au atoms to V, as the latter is always negatively charged in $Au_nV$ (see Table 3). In general, the natural charge of V decreases monotonically, demonstrating that V can play as an electron acceptor owing to its empty 3d orbitals. Electron donation comes from a combination of the d orbitals of vanadium with those of the gold framework. Hence, it is more effective if V is endohedrally confined and the host is large enough to accommodate the dopant.

An interesting point to be mentioned is that V receives a more negative charge with increasing gold cluster size. This means that the $Au_n$ framework becomes more electropositive in the larger sizes. In this context, the electronegativity for gold clusters can be estimated from the experimental ionization energy (IE) and electron affinity (EA) values by using the Mulliken formula, namely:

$$EN = 0.187(IE + EA).$$

We find that (*cf.* results listed in Table S2 of the ESI†) the electronegativity is marginally changed with respect to the cluster size. For example, the predicted values for $Au_2$ and $Au_3$ are around 2.14 and 2.13 eV as compared to 2.17 and 2.05 eV of $Au_{13}$ and $Au_{14}$. The presence of V thus substantially improves the ability to donate electrons of a gold cluster irrespective of the resulting electronegativity.

As mentioned above, the optimal structure of $Au_nV$ at a certain size is normally generated from that of the smaller one by adding an extra gold atom. Accordingly, the energy gain in incorporating an Au atom to the smaller size is called the embedding energy (EE). It can also be considered as the energy needed to detach one gold atom from $Au_nV$, giving rise to $Au_{n-1}V$. The EEs for $Au_nV$ clusters calculated at the BP86/cc-pVTZ-PP + ZPE level are plotted in Fig. 4.

Among the $Au_nV$ species considered, $Au_2V$ and $Au_{11}V$ are characterized by the highest EE values, implying a particular thermodynamic stability even though they have an open-shell electronic structure. The calculated EE value of $Au_2V$ is *ca.* 2.8 eV as compared to 2.7 and 2.3 eV of AuV and $Au_3V$, respectively. The trimer is found to be especially stable since both Au and V are expected to fulfill their outer shells, in which V donates two electrons for making chemical bonds. A similar trend was also observed for $Au_2Mn$, $Au_2Fe$, and $Au_2Zn$.[67–69] However, $Au_2Cr$ and $Au_2Ag$ were found to be extremely unstable,[53,70] as chromium and silver are willing to provide only one electron to the utmost orbital. Equally stable are the clusters at $n$ = 6, 11, 12 and 14. In contrast, the super-atomic molecule $Au_{13}V$ holds rather low dissociation energy. It is worth noting that $Au_6V$, $Au_{12}V$ and $Au_{14}V$ possess an odd number of electrons. Accordingly, their stability could be due to a dominant geometric effect, in which the stability is

 

determined more by the number of atoms rather than by the number of electrons. In other words, these clusters are stabilized as they can form a compact symmetric structure yielding an enhanced stability.[71] In fact, as discussed above, $Au_6V$ is slightly distorted from a $D_{6h}$ form whereas $Au_{12}V$ is nearly a cuboctahedron and $Au_{14}V$ has a high $D_{2d}$ symmetry.

For the sake of comparison, the EE values of pure gold clusters up to $Au_{15}$, re-calculated at the BP86/cc-pVTZ-PP + ZPE level, are also displayed in Fig. 4, along with those of $Au_nV$ clusters. It is clearly reflected in Fig. 4 that the EEs of the smallest pure clusters, *i.e.* $Au_2$ and $Au_3$, are much smaller than those of AuV and $Au_2V$. This indicates that a chemical bond between Au and V is stronger than that between Au atoms. Regarding the larger systems, replacement of Au by V greatly increases the stability of $Au_n$ with odd number $n$. In contrast, a reverse result holds true for even-numbered size systems. For instance, the EEs of $Au_{12}$ and $Au_{13}$ are 2.9 and 1.9 eV, respectively, as compared to 2.7 and 2.6 eV of $Au_{11}V$ and $Au_{12}V$. These observations lend support for a view that in addition to one delocalized 6s electron from each Au atom, each V atom contributes two 4s delocalized electrons and zero 3d delocalized electrons to form electronic shells.[42] However, it should be stressed that the number of delocalized electrons depends on both the behaviour of constituent atoms and cluster shape.[72]

The second-order difference of energy ($\Delta^2E$) is additionally an important indicator that measures the relative stability of clusters. In particular, peaks in the graph of $\Delta^2E$ as a function of cluster sizes were found to be correlated well with peaks in the experimental mass spectra.[73] As illustrated in Fig. 4, our calculations show local maxima at $n$ = 2, 4, 7, 9, 11 and 12, implying that these clusters are more stable than their immediate neighboring ones. However, the energy difference between them is not very large. This is also in agreement with the analysis based on embedding energies given above. For a pure gold system (*cf.* Fig. 4), there exist extreme odd–even fluctuations, in that a cluster with an even number of atoms is more stable than the odd-numbered ones. In agreement with the above analysis based on the embedding energies, replacing an Au atom in odd-numbered gold clusters by vanadium element invariably enhances the system stability. A reverse fashion also holds true for the even-numbered gold clusters. Thus, doping a gold cluster with impurity causes significant changes in the magic numbers because their electronic shell structure is strongly affected.[74]

### 3.D. Other thermochemical properties

Basic thermochemical properties of pure gold clusters such as electron affinities (EA) and ionization energies (IE) have extensively been investigated using both experimental and theoretical approaches.[3,10,13,15,40,75–78] In contrast, there have been only a few studies on such properties of $Au_nV$, and most of them were carried out for a few specific sizes.[28,38,40] In the present work, we systematically evaluate the vertical and adiabatic detachment energies for anions $Au_nV^-$ in the same range of size $n$ = 1–14, using the same BP86/cc-pVTZ-PP level (Table 2).

The vertical detachment energies (VDEs) of anions are calculated at the anion geometry, whereas the adiabatic detachment energies (ADEs) refer to the values obtained using the optimized structures of both neutral and anionic forms. Furthermore, we computed the vertical ionization energies (VIEs) of neutral clusters by taking the geometry of vertical cations to be the same as neutral counterparts.

**Table 2** Ionization energies of $Au_nV$ clusters and detachment energies of $Au_nV^-$ clusters ($n$ = 1–14) computed at the BP86/cc-pVTZ-PP level

| $n$ | Vertical ionization energies[a]/eV | Detachment energies/eV | |
|---|---|---|---|
| | | ADEs | VDEs |
| 1 | 7.30 [9.58] | 1.17 | 1.23 |
| 2 | 8.35 [8.53] | 1.82 | 1.97 |
| 3 | 8.16 [8.05] | 2.60 | 2.87 |
| 4 | 7.51 [7.64] | 2.82 | 3.39 |
| 5 | 7.38 [8.23] | 2.78 | 2.86 |
| 6 | 7.60 [7.27] | 3.29 | 3.40 |
| 7 | 7.24 [7.92] | 2.91 | 2.92 |
| 8 | 6.99 [7.13] | 3.05 | 3.12 |
| 9 | 7.28 [7.59] | 3.24 | 3.26 |
| 10 | 7.05 [6.40] | 3.31 | 3.59 |
| 11 | 7.12 [7.40] | 3.19 | 3.32 |
| 12 | 6.81 [7.00] | 3.20 | 3.85[b] |
| 13 | 6.83 [7.46] | 3.34 | 3.54 |
| 14 | 7.07 [6.86] | 3.31 | 3.40 |

[a] VIEs of $Au_{n+1}$ are given in square brackets. [b] The values computed with the LanL2DZ basis set.

The odd/even alternations of IEs and EAs are typically found in metal clusters with an odd number of electrons per atom such as Na, Al and Nb,[79–81] and so are clusters of gold.[26,78,82] On the other hand, such patterns are not clearly observed for gold-doped vanadium clusters. As presented in Table 1, the ADEs, which are also the EAs of neutral species, increase gradually with respect to cluster sizes. For example, the ADEs of AuV and $Au_2V$ are 1.2 and 1.8 eV as compared to 3.3 and 3.3 eV of $Au_{13}V$ and $Au_{14}V$, respectively. The VDEs of anions also exhibit a similar trend. Especially, both vertical and adiabatic detachment energies increase drastically from $Au_2V$ to $Au_3V$. This observation reflects the emergence of an electron transfer from Au to V in clusters larger than $Au_2V$, leading to a more positive charge of gold skeletons. In fact, the natural charge of V in AuV and $Au_2V$ species is much more positive than that of V in larger species (see Table 3). It is in addition noticeable that the anions with $n$ = 6, 9, 10, 12 and 13 have larger electron detachment energies than the others, while the tetrahedron $Au_4V^-$ holds the highest VDE among the smaller sizes. Moreover, the difference between the vertical and adiabatic EAs of clusters with $n$ = 4, 10, and 12 is much larger because of the large differences between the lowest-energy structures for these anions and neutrals, as mentioned above.

Previously, Li *et al.*[29] measured the photoelectron spectra of $Au_6V^-$ and evaluated its VDE and ADE values around 3.25 ± 0.02 and 3.23 ± 0.02 eV, respectively. The corresponding BP86/cc-pvTZ-PP value of ADE = 3.29 eV is thus in good agreement, but the VDE counterpart of 3.40 eV is somewhat overestimated. As reported in ref. 28, the icosahedral anion $Au_{12}V^-$ is characterized by a measured VDE of *ca.* 3.79 eV, which is not only larger than that of "super-halide" $Al_{13}^-$ (~3.57 eV)[83] but also even larger than that of the chloride anion (3.61 eV).[84] Our calculated VDE and ADE of $Au_{12}V^-$ amount to 3.20 and 3.85 eV, respectively. The calculated VDE

**Table 3** Natural charges (a.u.) distributed on V of $Au_nV$ clusters ($n$ = 1–14) computed using two different functionals with the cc-pVTZ-PP basis set

| | NBO charges | |
|---|---|---|
| Isomers | BP86 | M06 |
| **1–I** | 0.42 | 0.56 |
| **2–I** | 0.64 | 0.62 |
| **3–I** | 0.23 | 0.22 |
| **4–I** | 0.26 | 0.23 |
| **5–I** | −0.16 | −0.26 |
| **6–I** | −0.41 | −0.56 |
| **7–I** | −0.31 | −0.39 |
| **8–I** | −0.09 | −0.12 |
| **9–I** | −1.62 | −1.61 |
| **10–I** | −1.98 | −1.98 |
| **10–III** | −3.32 | −3.31 |
| **11–I** | −3.59 | −3.66 |
| **12–I** | −4.37 | −4.45 |
| **13–I** | −4.93 | −5.13 |
| **13–II** | −4.04 | −4.12 |
| **14–I** | −4.53 | −4.60 |
| **14–II** | −4.45 | −4.52 |

of $Au_{12}V^-$ is thus compared well with the experimental value of 3.79 eV, but the corresponding ADE of 3.20 eV appears underestimated as compared to the experimental estimate of 3.70 eV. Nevertheless, in addition to the intense band centered at around 3.70 eV, Zhai *et al.*[28] also found that the photoelectron spectrum of $Au_{12}V^-$ exhibits a low intensity peak at a lower binding energy of ~3.20 eV. The origin of this peak can either be contaminations or structural isomers. Indeed, the VDE of the cuboctahedral isomer is computed to be 3.21 eV.

The particularly large VDE indicates that $Au_{12}V^-$ is unwilling to loose electron as, in terms of the modified phenomenological shell model,[74] it has a closed-shell structure with a configuration [$1S^21P^61D^{10}$]. The anion is expected to have 18 valence electrons because, in addition to one delocalized 6s electron from each gold atom, it is assumed to have five delocalized electrons on 4s and 3d orbitals of vanadium. Moreover, the exceptional stability and a spherical aromaticity for $Au_{12}V^-$ are likely due to the simple fact that the well-known 18-electron rule[85] of d elements is here satisfied. Recently, Pyykkö and Runeberg[27] predicted the existence of $Au_{12}W$ with a huge frontier orbital gap of 3.0 eV (B3LYP/LanL2DZ). However, Li *et al.*[29] evaluated from their experiment a much smaller value of 1.68 eV, which is comparable to the measured gap of 1.77 eV in the magic cluster $Au_{20}$.[8]

Due to the smaller electron affinity of vanadium as compared to that of gold, AuV is much easier to oxidize than $Au_2$. In fact, the former has a predicted VIE of 7.3 eV as compared to 9.6 eV of $Au_2$. NBO analysis shows a net charge of V in $AuV^+$ to be +1.1 electron as compared to +0.4 electron of V in AuV. Forming cations from larger neutral clusters, on the contrary, causes a little change of the vanadium charge (*cf.* Table S1 of the ESI†). As a result, their VIEs arise from the external gold cages. The VIEs of impure clusters $Au_nV$ and the pure counterparts $Au_{n+1}$ are not much different from each other. Up to the size $n$ = 5, $Au_nV$ clusters are still somewhat easier to oxidize than the corresponding pure $Au_{n+1}$. For clusters larger than $n$ = 5, replacement of Au by V invariably increases IEs of odd-numbered pure clusters, and decreases those of even-numbered systems. For example, the computed VIEs of $Au_{10}V$ and $Au_{11}V$ are 7.0 and 7.1 eV, while those of $Au_{11}$ and $Au_{12}$ are 6.4 and 7.4 eV, respectively. However, some exceptions include $Au_8V$ and $Au_{12}V$ as their VIEs are smaller than those of their counterparts $Au_9$ and $Au_{13}$. Among the larger sizes, $Au_6V$ has the highest VIE, indicating its higher thermodynamic stability.

Fig. 5 and 6 show the shapes and symmetries of valence MOs for $Au_6V$ and $Au_{12}V$ systems. The chemical bonding in both clusters is analogous to the homoleptic complexes in which V plays as a central atom surrounded by the gold frameworks. As illustrated in Fig. 5, when placed at the center of an $Au_6$ ring, five d orbitals of V are no longer degenerate. Instead they split into five un-equivalent orbitals with $b_{3g}$, $b_{1g}$, $b_{2g}$, $1a_g$ and $2a_g$ sub-symmetries of the $D_{2h}$ group, in which the $b_{3g}$ orbital is doubly occupied, the three orbitals $b_{1g}$, $b_{2g}$, $1a_g$ are singly occupied, and the $2a_g$ being the LUMO. The primary orbital interactions occur between the valence orbitals of V and π/δ orbitals of the $Au_6$ ring, giving rise to the orbital configuration $\ldots b_{1u}^2 b_{3g}^2 b_{2u}^2 b_{3g}^2 b_{1g}^1 b_{2g}^1 1a_g^1$. Due to the difference in energy, the HOMO-4 ($b_{2u}$), HOMO-5 ($b_{3g}$) and HOMO-6 ($b_{1u}$) are mainly ligand based and the valence electrons from the $Au_6$ ring enter into these orbitals, thus leaving $b_{3g}$, $b_{1g}$, $b_{2g}$ and $a_g$ orbitals to accommodate the valence electrons from the V atom.

As compared to the $Au_6$ ring, the linear combinations of V d orbitals with the π/δ-orbitals of the $Au_{12}$ cage are much more effective. In $Au_6V$, three of five V d orbitals remain nonbonding,

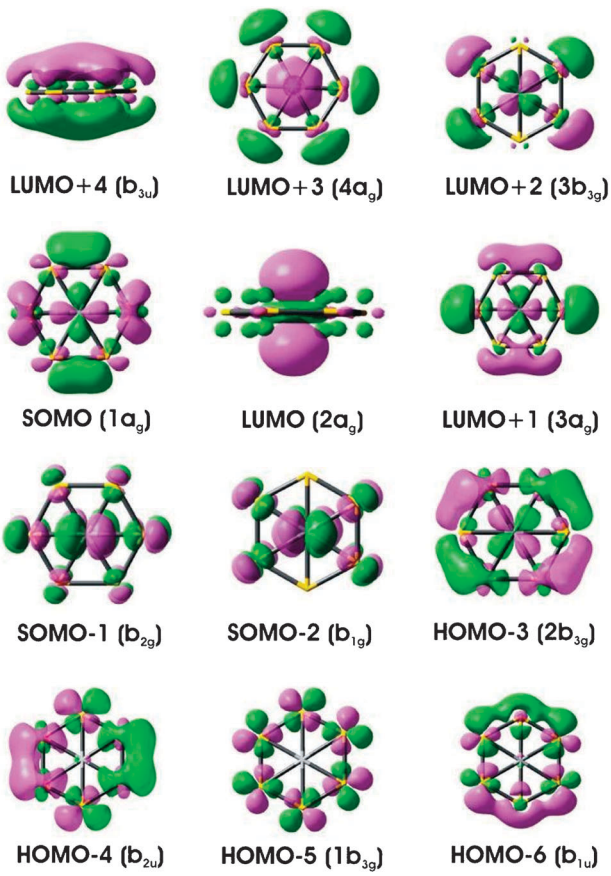


**Fig. 5** Shapes and symmetries of valence MOs for $Au_6V$.

 

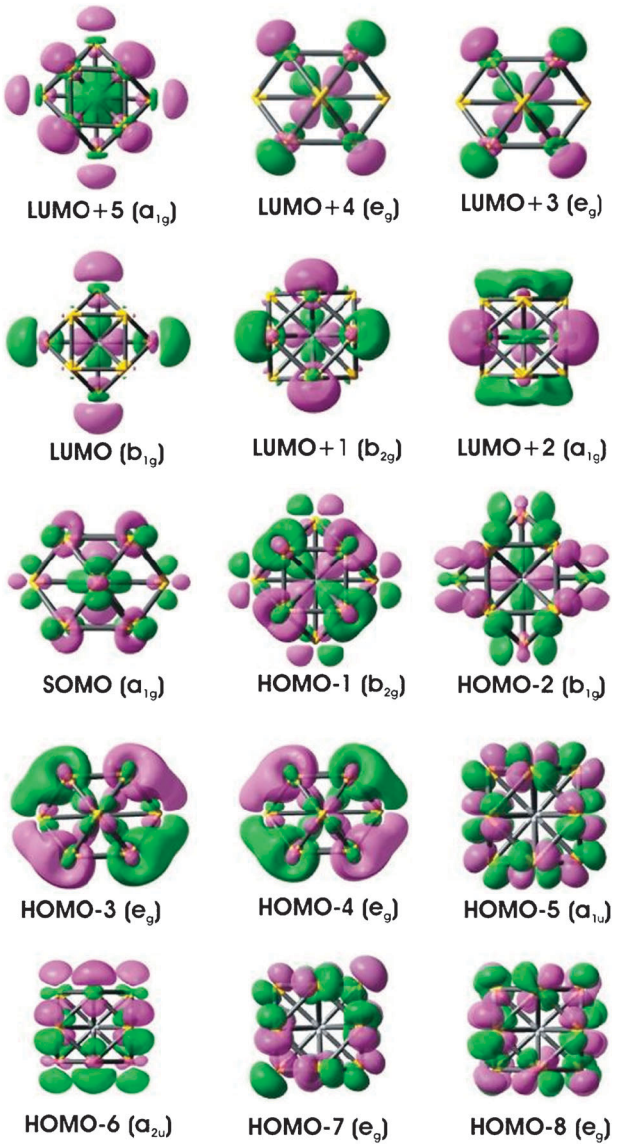


**Fig. 6** Shapes and symmetries of valence MOs for $Au_{12}V$.

while all five V d orbitals become bonding in $Au_{12}V$. The orbitals up to HOMO-3 ($e_g$) are filled by valence electrons of the $Au_{12}$ skeleton, and the valence electrons from V are filled starting from $b_{1g}$ (HOMO-2). The doubly degenerate $e_g$ orbitals (HOMO-3 and HOMO-4) are formed from the $d_{xz}$, $d_{yz}$ AOs and δ orbitals of the $Au_{12}$ cage with $E_g$ symmetry. In addition, these MOs play the role as acceptors of electron transferred from gold atoms. As a result, V holds a highly negative charge in $Au_{12}V$ (−4.4 electron). The overlap between other V d AOs, *i.e.* $d_{xz}$, $d_{x2-y2}$ and $d_{z2}$, and the $Au_{12}$ orbitals with the same symmetries yields the $b_{1g}$, $b_{2g}$ and $a_{1g}$ orbitals. They are all bonding MOs and their corresponding antibonding counterparts also have been found (see Fig. 6).

## 4. Concluding remarks

In this theoretical study, we perform a systematic investigation on the electronic, geometric and energetic properties of bimetallic $Au_nV$ clusters with the size $n$ going up to 14, in both neutral and anionic states, using the BP86 functional in conjunction with the pseudo-potential basis set cc-pVTZ-PP. The effects of the dopant atom are analyzed in detail. All neutral clusters with an even number of electrons prefer a high spin state, namely a quintet state for AuV and triplet state for others with an exception of the $^1A'$ ground state for $Au_{13}V$. For odd-electron systems, a quartet state is invariably favoured as a ground state up to $Au_8V$. The larger sizes, *i.e.* $Au_{10}V$, $Au_{12}V$ and $Au_{14}V$, prefer a low spin (doublet) state.

Concerning the growth mechanism, we can now draw some key points. The clusters prefer 2D geometries up to $Au_8V$ involving a weak charge transfer. In contrast, the larger systems bear 3D conformations with a more effective electron transfer from gold atoms to vanadium. In general, the lowest-energy isomer of an $Au_nV$ species is built upon the most stable form of $Au_{n-1}V$. Another important observation is that during the growth, vanadium is always endohedrally doped as a way of maximizing its coordination numbers and augmenting the charge transfer.

Analyses of energetic properties including the BEs, EEs, and $\Delta^2E$ demonstrate that the presence of the V atom enhances considerably the thermodynamic stability of odd-numbered pure clusters but tends to reduce that of even-numbered systems. The atomic shapes have an apparently more important effect on the clusters stability than the electronic structure. Even though $Au_2V$, $Au_6V$, $Au_{12}V$, $Au_{14}V$ possess an odd number of electrons, they are rather stable due to their ability to form compact symmetric structures. Especially, if both atomic shape and electronic conditions are satisfied, the resulting cluster becomes particularly stable such as the anion $Au_{12}V^-$, which can thus combine with the cation $Au^+$ to form the superatomic molecule of the type $[Au_{12}V]Au$.

As in other transition metal clusters, multiple lower-lying electronic states of these clusters are lying very close in energy, in such a way that DFT computations cannot clearly establish their ground electronic states. Calculated results demonstrate the existence of structural isomers with comparable energy content for several species such as $Au_9V$, $Au_{10}V$, $Au_{13}V$ and $Au_{14}V$. We hope that these theoretical information would stimulate experimental studies on these interesting binary metal clusters.

## Acknowledgements

The authors are indebted to the KULeuven Research Council for continuing support *via* the programs GOA, IDO and IUAP. PVN is grateful to the University of Cantho for a partial doctoral scholarship. MTN thanks the ICST for supporting his stay in Vietnam.

## References

1 P. Schwerdtfeger, *Angew. Chem., Int. Ed.*, 2003, **42**, 1892.
2 M. Haruta, *Catal. Today*, 1997, **36**, 153.
3 K. J. Taylor, C. L. Pettiette-Hall, O. Cheshnovsky and R. E. Smalley, *J. Chem. Phys.*, 1992, **96**, 3319.
4 J. Ho, K. M. Ervin and W. C. Lineberger, *J. Chem. Phys.*, 1990, **93**, 6987.
5 H. Handschuh, G. Ganteför, P. S. Bechthold and W. Eberhardt, *J. Chem. Phys.*, 1994, **100**, 7093.

6 K. Hansen, A. Herlert, L. Schweikhard and M. Vogel, *Phys. Rev. A*, 2006, **73**, 063202.
7 P. Gruene, D. M. Rayner, B. Redlich, A. F. G. van der Meer, J. T. Lyon, G. Meijer and A. Fielicke, *Science*, 2008, **321**, 674.
8 J. Li, X. Li, H. J. Zhai and L. S. Wang, *Science*, 2003, **299**, 864.
9 X. B. Li, H. Y. Wang, X. D. Yang, Z. H. Zhu and Y. J. Tang, *J. Chem. Phys.*, 2007, **126**, 084505.
10 E. M. Fernández, J. M. Soler, I. L. Garzón and L. C. Balbás, *Phys. Rev. B: Condens. Matter*, 2004, **70**, 165403.
11 S. Gilb, P. Weis, F. Furche, R. Ahlrichs and M. M. Kappes, *J. Chem. Phys.*, 2002, **116**, 4094.
12 H. Woldeghebriel and A. Kshirsagar, *J. Chem. Phys.*, 2007, **127**, 224708.
13 F. Furche, R. Ahlrichs, P. Weis, C. Jacob, S. Gilb, T. Bierweiler and M. M. Kappes, *J. Chem. Phys.*, 2002, **117**, 6982.
14 M. P. Johansson, A. Lechtken, D. Schooss, M. M. Kappes and F. Furche, *Phys. Rev. A*, 2008, **77**, 053202.
15 B. Assadollahzadeh and P. Schwerdtfeger, *J. Chem. Phys.*, 2009, **131**, 064306.
16 L. Ferrighi, B. Hammer and G. K. H. Madsen, *J. Am. Chem. Soc.*, 2009, **131**, 10605.
17 P. Pyykkö, *Angew. Chem., Int. Ed.*, 2004, **43**, 4412.
18 P. Pyykkö, *Chem. Rev.*, 1988, **88**, 563.
19 P. A. Christiansen, W. C. Ermler and K. S. Pitzer, *Annu. Rev. Phys. Chem.*, 1985, **36**, 407.
20 P. Pyykkö, *Inorg. Chim. Acta*, 2005, **358**, 4113.
21 P. Pyykkö, *Chem. Soc. Rev.*, 2008, **37**, 1967.
22 P. Schwerdtfeger, *Heteroat. Chem.*, 2002, **13**, 578.
23 C. Majumder, *Phys. Rev. B: Condens. Matter*, 2007, **75**, 235409.
24 B. Kiran, X. Li, H. J. Zhai, L. F. Cui and L. S. Wang, *Angew. Chem., Int. Ed.*, 2004, **43**, 2125.
25 C. Majumder, A. K. Kandalam and P. Jena, *Phys. Rev. B: Condens. Matter*, 2006, **74**, 205437.
26 H. Häkkinen, *Chem. Soc. Rev.*, 2008, **37**, 1847.
27 P. Pyykkö and N. Runeberg, *Angew. Chem., Int. Ed.*, 2002, **41**, 2174.
28 H. J. Zhai, J. Li and L. S. Wang, *J. Chem. Phys.*, 2004, **121**, 8369.
29 X. Li, B. Kiran, J. Li, H. J. Zhai and L. S. Wang, *Angew. Chem., Int. Ed.*, 2002, **41**, 4786.
30 J. Autschbach, B. A. Hess, M. P. Johansson, J. Neugebauer, M. Patzschke, P. Pyykkö, M. Reiher and D. Sundholm, *Phys. Chem. Chem. Phys.*, 2004, **6**, 11.
31 J. Graciani, J. Oviedo and J. F. Sanz, *J. Phys. Chem. B*, 2006, **110**, 11600.
32 H. Häkkinen, B. Yoon, U. Landman, X. Li, H. J. Zhai and L. S. Wang, *J. Phys. Chem. A*, 2003, **107**, 6168.
33 Y. Gao, S. Bulusu and X. C. Zeng, *J. Am. Chem. Soc.*, 2005, **127**, 15680.
34 L. M. Wang, S. Bulusu, H. J. Zhai, X. C. Zeng and L. S. Wang, *Angew. Chem., Int. Ed.*, 2007, **46**, 2915.
35 L. M. Wang, J. Bai, A. Lechtken, W. Huang, D. Schooss, M. M. Kappes, X. C. Zeng and L. S. Wang, *Phys. Rev. B: Condens. Matter*, 2009, **79**, 033413.
36 L. M. Wang, R. Pal, W. Huang, X. C. Zeng and L. S. Wang, *J. Chem. Phys.*, 2009, **130**, 051101.
37 L. Lin, P. Claes, P. Gruene, G. Meijer, A. Fielicke, M. T. Nguyen and P. Lievens, *ChemPhysChem*, 2010, **11**, 1932.
38 X. Li, B. Kiran, L. F. Cui and L. S. Wang, *Phys. Rev. Lett.*, 2005, **95**, 253401.
39 M. Zhang, L. M. He, L. X Zhao, X. J. Feng and Y. H. Luo, *J. Phys. Chem. C*, 2009, **113**, 6491.
40 M. Stener, A. Nardelli and G. Fronzoni, *Chem. Phys. Lett.*, 2008, **462**, 358.
41 A. Yang, W. Fa and J. Dong, *J. Phys. Chem. A*, 2010, **114**, 4031.
42 M. B. Torres, E. M. Fernández and L. C. Balbás, *Phys. Rev. B: Condens. Matter*, 2005, **71**, 155412.
43 M. J. Frisch, *et al.*, *Gaussian 09 Revision: B.01*, Gaussian, Inc., Wallingford, CT, 2009.
44 K. A. Peterson, D. Figgen, E. Goll, H. Stoll and M. Dolg, *J. Chem. Phys.*, 2003, **119**, 11113.
45 M. D. Morse, *Chem. Rev.*, 1986, **86**, 1079.
46 V. B. Koutecký, J. Burda, R. Mitrić, M. Ge, G. Zampella and P. Fantucci, *J. Chem. Phys.*, 2002, **117**, 3120.
47 C. J. Cramer and D. G. Truhlar, *Phys. Chem. Chem. Phys.*, 2009, **11**, 10757.
48 C. J. Barden, J. C. Rienstra-Kiracofe and H. F. Schaefer III, *J. Chem. Phys.*, 2000, **113**, 690.
49 S. Li and D. A. Dixon, *J. Phys. Chem. A*, 2007, **111**, 11908.
50 C. Diedrich, A. Luchow and S. Grimme, *J. Chem. Phys.*, 2005, **122**, 021101.
51 F. Stevens, I. Carmichael, F. Callens and M. Waroquier, *J. Phys. Chem. A*, 2006, **110**, 4846.
52 P. Song, W. Guan, C. Yao, Z. Su, Z. Wu, J. Feng and L. Yan, *Theor. Chem. Acc.*, 2007, **117**, 407.
53 H. M. Lee, M. Ge, B. R. Sahu, P. Tarakeshwar and K. S. Kim, *J. Phys. Chem. B*, 2003, **107**, 9994.
54 L. Xiao, B. Tollberg, X. Hu and L. Wang, *J. Chem. Phys.*, 2006, **124**, 114309.
55 J. C. Idrobo, W. Walkosz, S. F. Yip, S. Ögut, J. Wang and J. Jellinek, *Phys. Rev. B: Condens. Matter*, 2007, **76**, 205422.
56 Y. Han, *J. Chem. Phys.*, 2006, **124**, 024316.
57 (*a*) T. Höltzl, P. Lievens, T. Veszprémi and M. T. Nguyen, *J. Phys. Chem. C*, 2009, **113**, 21016; (*b*) T. Höltzl, N. Veldeman, J. De Haeck, T. Veszprémi, P. Lievens and M. T. Nguyen, *Chem.–Eur. J.*, 2009, **15**, 3970.
58 M. X. Chen and X. H. Yan, *J. Chem. Phys.*, 2008, **128**, 174305.
59 C. Barreteau, M. C. Desjonqueres and D. Spanjaard, *Eur. Phys. J. D*, 2000, **11**, 395.
60 J. Long, Y. X. Qiu, X. Y. Chen and S. G. Wang, *J. Phys. Chem. C*, 2008, **112**, 12646.
61 K. Jug, B. Zimmermann, P. Calaminizi and A. Köster, *J. Chem. Phys.*, 2002, **116**, 4497.
62 T. Höltzl, N. Veldeman, J. D. Haeck, T. Veszprémi, P. Lievens and M. T. Nguyen, *Chem.–Eur. J.*, 2009, **15**, 3970.
63 M. X. Chen and X. H. Yan, *J. Chem. Phys.*, 2008, **128**, 174305.
64 J. Wang, G. Wang and J. Zhao, *Phys. Rev. B: Condens. Matter*, 2002, **66**, 035418.
65 P. Schwerdtfeger, M. Dolg, W. H. E. Schwarz, G. A. Bowmaker and P. D. W. Boyd, *J. Chem. Phys.*, 1989, **91**, 1762.
66 P. Schwerdtfeger and M. Dolg, *Phys. Rev. A*, 1991, **43**, 1644.
67 D. Die, X. Y. Kuang, J. J. Guo and B. X. Zheng, *THEOCHEM*, 2009, **902**, 54.
68 D. Die, X. Y. Kuang, J. J. Guo and B. X. Zheng, *J. Phys. Chem. Solids*, 2010, **71**, 770.
69 H. Tanaka, S. Neukermans, E. Janssens and R. E. Silverans, *J. Chem. Phys.*, 2003, **119**, 14.
70 D. Die, X. Y. Kuang, J. J. Guo and B. X. Zheng, *Physica A (Amsterdam)*, 2010, **389**, 5216.
71 T. P. Martin, *Phys. Rep.*, 1996, **273**, 199.
72 E. Janssens, H. Tanaka, S. Neukermans, R. E. Silverans and P. Lievens, *Phys. Rev. B: Condens. Matter*, 2004, **69**, 085402.
73 F. Baletto and R. Ferrando, *Rev. Mod. Phys.*, 2005, **77**, 371.
74 E. Janssens, S. Neukermans and P. Lievens, *Curr. Opin. Solid State Mater. Sci.*, 2004, **8**, 185.
75 M. A. Cheeseman and J. R. Eyler, *J. Phys. Chem.*, 1992, **96**, 1082.
76 C. Jackschath, I. Rabin, W. Schulze and B. Bunsenges, *J. Phys. Chem.*, 1992, **96**, 1200.
77 *CRC Handbook of Chemistry and Physics*, ed. D. R. Linde, CRC, Boca Raton, 2002.
78 X. B. Li, H. Y. Wang, X. D. Yang, Z. H. Zhu and Y. J. Tang, *J. Chem. Phys.*, 2007, **126**, 084505.
79 W. A. de Heer, *Rev. Mod. Phys.*, 1993, **65**, 611.
80 C. Y. Cha, G. Gantefor and W. Eberhardt, *J. Chem. Phys.*, 1994, **100**, 995.
81 P. V. Nhat, V. T. Ngan, T. B. Tai and M. T. Nguyen, *J. Phys. Chem. A*, 2011, **115**, 3523.
82 H. Häkkinen and U. Landman, *Phys. Rev. B: Condens. Matter*, 2000, **62**, 0163.
83 X. Li and L. S. Wang, *Phys. Rev. B: Condens. Matter*, 2000, **65**, 153404.
84 D. R. Lide, *CRC Handbook of Chemistry and Physics*, 73rd edn, CRC Press, Boca Raton, FL, 1992.
85 I. Langmuir, *Science*, 1921, **54**, 59.


 